Article

# Identification of a Fe-Dependent Optical Mode in CuAl$_{1-x}$Fe$_x$O$_2$

Mina Aziziha, Saeed Akbarshahi, Suresh Pittala, Sayandeep Ghosh, Rishmali Sooriyagoda,
Aldo H. Romero, Subhash Thota, Alan D. Bristow, Mohindar S. Seehra, and Matthew B. Johnson*

ACCESS | 📊 Metrics & More | 📖 Article Recommendations

**ABSTRACT:** Delafossites are promising candidates for photocatalysis applications because of their chemical stability and absorption in the solar region of the electromagnetic spectrum. For example, CuAlO$_2$ has good chemical stability but has a large indirect band gap, so that efforts to improve its absorption in the solar region through alloying are investigated. The effect of dilute alloying on the optical absorption of powdered CuAl$_{1-x}$Fe$_x$O$_2$ ($x = 0.0-1.0$) is measured and compared to electronic band structures calculations using a generalized gradient approximation with Hubbard parameter and spin. A new absorption feature is observed at 1.8 eV for $x = 0.01$, which red-shifts to 1.4 eV for $x = 0.10$. This feature is associated with transitions from the L-point valence band maximum to the Fe-3d state that appears below the conduction band of the spin-down band structure. The feature increases the optical absorption below the band gap of pure CuAlO$_2$, making dilute CuAl$_{1-x}$Fe$_x$O$_2$ alloys better suited for solar photocatalysis.
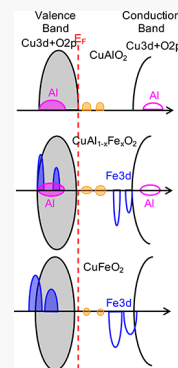
## INTRODUCTION

A potential photocatalyst should have high quantum efficiency and be chemically stable. Ideally, they should be simple to synthesize and have a good surface-to-volume ratio. Metal oxides such as delafossite (ABO$_2$) crystals have attracted attention because of their chemical stability during electrolysis[1−6] and a tendency for native p-type doping and often with small indirect gaps ($E_g < 1.5$ eV) which makes them into good conducting electrodes.[7−9] Delafossite crystals, such as CuAlO$_2$, have wide indirect and direct optical band gaps ($E'_g = 3.0$ and 3.8 eV, respectively), exhibit a large exciton binding energy, and have strong lattice polarization.[10−16] Moreover, in the powdered form, there are surface states that add to the optical spectrum without necessarily offering useful charges for photocatalysis.[14] The optical absorption needs to be increased in the visible/solar range of the electromagnetic spectrum specifically to improve photocatalytic activity. As has been shown in CuGaO$_2$,[17] a promising way to do this is to alloy CuAlO$_2$ with smaller optical band gap delafossites, such as CuFeO$_2$ ($E'_g \approx 2.1$ eV).[18] In principle, dilute CuAl$_{1-x}$Fe$_x$O$_2$ should break symmetry of the pure CuAlO$_2$ sufficiently to lower the band edge and create better photocatalytic absorption.

The calculation of the electronic band structure and the resultant optical absorption for pure nonalloyed delafossites is already challenging. Density functional theory (DFT), using local density (LDA) and generalized gradient (GGA) approximations, successfully predicts the crystal geometry of the insulators. However, they usually fail to predict the insulating band structure of transition-metal oxides such as CuAlO$_2$[8,19−21] because they underestimate d-orbital correlations.[22] This can be overcome by including a Hubbard parameter (DFT+$U$)[23,24] or Green's function with Coulomb screening (GW),[12,15] both of which are more suitable for calculations of d orbitals.[25−28] Calculations using LDA/GGA+$U$ correct the energy of the d orbitals through the $U$ parameter, which is itself not self-interaction-free. These oxides exhibit strong polaronic (large polaron constant: $\alpha_p \sim 1$[11]) and excitonic effects (exciton binding energy of ~0.5 eV[15]) that can be modeled in GW calculations with a many-body quasi-particle approach. Alternatively, hybrid functional calculations can mostly fix the self-interaction problem, improve the treatment of localized states, and better predict the band gap.[29] However, hybrid functionals are more computationally demanding than DFT+$U$ calculations for delafossites, and these demands are greater still when extending the calculations to dilute alloys that require large supercells, not one unit cell. For example, one Fe atom in a $3 \times 3 \times 3$ supercell is 4% Fe concentration (CuAl$_{0.96}$Fe$_{0.04}$O$_2$), whereas changes are expected to be observed for dilute concentrations at and below 1%. For practical reasons, taking a GGA+$U$ approach for dilute alloys of CuAl$_{1-x}$Fe$_x$O$_2$ will handle the charge distribution of the d orbitals and make use of well-established values of $U$[25] and can be applied across a wide concentration range.
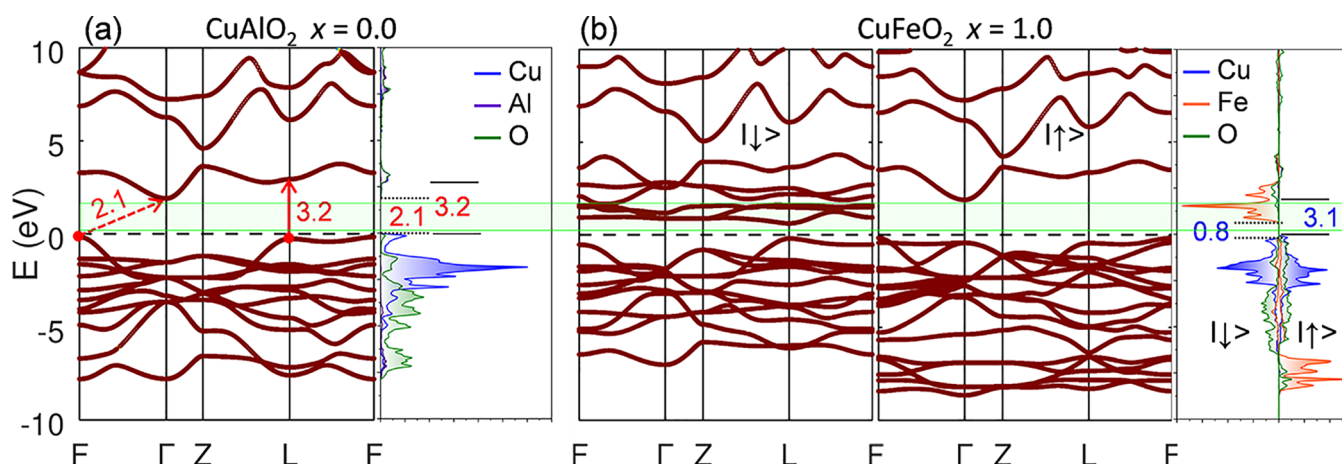
**Figure 1.** (a) Electronic band structure of $CuAlO_2$ with the density of states alongside. (b) Electronic band structure of the $CuFeO_2$ spin-down ($|\downarrow\rangle$) on left spin-up ($|\uparrow\rangle$) on right, as labeled, with density of states alongside. The black dashed lines show the Fermi energy. A shaded rectangle highlights the energy region where there are no states in $CuAlO_2$ and closely spaced states in $CuFeO_2$.

The delafossite $CuAlO_2$ has good chemical stability but has a large indirect band gap (~3 eV), so that efforts to improve its absorption in the solar region through alloying are investigated. Specifically, a comparison of optical absorption spectra and computed band structures is presented for the dilute alloys $CuAl_{1-x}Fe_xO_2$ ($x$ = 0.0–0.10) and $CuFeO_2$ ($x$ = 1.0). First-principles DFT calculations are performed to obtain the electronic band structure, and powdered alloys are measured in the photon energy range of 1−6 eV. Although powder samples exhibit pronounced defects, the consistent presence of the higher energy indirect and direct band gaps associated with the $CuAlO_2$ is observed at 3.2 and 3.8 eV, respectively. A new lower-energy absorption line is observed at about 1.8 eV that is associated with the Fe-3d band, which appears within the calculated $CuAlO_2$ band gap. This Fe-3d absorption line is observed to red-shift with increasing Fe concentration. However, both experimentally observed and computed super-cell band structure results confirm the direct and indirect transitions do not change.

### METHOD

**Experiments.** $CuAl_{1-x}Fe_xO_2$ powders ($x$ = 0.0, 0.01, 0.05, and 0.10) were prepared by the solid-state reaction method using $Cu_2O$, $Al_2O_3$, and $\alpha$-$Fe_2O_3$ as precursors in calculated stoichiometric ratios with heat treatments in static air at 1100 °C.[30] The $x$ = 1.0 sample was synthesized in an ambient argon at 1000 °C. Details of this work, including structural, chemical, IR/phonon, and magnetic characterization, are given in recent papers.[31−34] The optical properties of these alloy powders in UV−visible−near-IR (UV−vis−NIR) of 1−6 eV were measured at room temperature by using diffuse reflectance spectroscopy employing a Shimadzu MPC3100 UV−vis spectrometer with an integrating sphere (using a $BaSO_4$ powder reference for background correction).

**Computations.** DFT calculations are performed by using the Vienna Ab initio Simulation Package (VASP),[35−37] with the generalized gradient approximation (GGA) exchange-correlation functional parametrized by Perdew, Burke, and Ernzerhof (PBE)[26] and projector-augmented wave (PAW) pseudopotentials[27] with the valence-electron configurations $3p^63d^{10}4s^1$, $3p^63d^74s^1$, $3s^23p^1$, and $2s^22p^4$ for Cu, Fe, Al, and O, respectively. A simplified rotationally invariant PBE+$U$ approach[38] is taken with an on-site Coulomb parameter $U_{eff}$

= 4.0 eV, as suggested by Jain et al.,[25] for both Fe and Cu. Spin polarization for Fe is also included. Structural relaxation is used, leaving the supercell volume, positions, and cell shape free to change. A 3 × 3 × 3 supercell is constructed from the rhombohedral structure ($R\bar{3}m$) primitive unit cell of the $CuAlO_2$ with 108 atoms to calculate comparable dilute alloys. There are many possible configurations for Fe substituting of Al, but most of them can be ruled out by symmetry using a site-occupation disorder (SOD) code.[39] The structural relaxation of the resulting disordered supercell uses a 4 × 4 × 4, Γ-centered, $k$-point grid, and for all calculations, the electron wave functions were expanded in a plane-wave basis set with cutoff kinetic energy set to 600 eV. The Fold2Bloch code[40,41] was employed to relate the supercell band structure to the primitive basis representation using Bloch spectral density.

### RESULTS AND DISCUSSION

Figure 1a shows the computed band structure and density of states (DOS) for $CuAlO_2$. The lowest conduction band (CB) consists of O-2p orbitals with a minimum located at Γ-point. The valence band (VB) consists of Cu-3d orbitals with maxima located at the L- and F-points. A direct optical band gap of 3.2 eV is marked in Figure 1a at the L-point, which is slightly lower than, but consistent with, other reported values (3.4−4.0 eV).[8,13,24,42,43] Similarly, there is a smaller indirect fundamental band gap ($E_g$ = 2.1 eV) between the VB maximum at the F-point and the CB minimum at Γ-point (see Figure 1a). This is slightly higher than earlier LDA/GGA calculations that calculate indirect band gaps between 1.6 and 2.0 eV,[7−9] but these earlier calculations without the addition of the Hubbard parameter are known to underestimate $E_g$. Any correspondence between such calculations and experimentally observed optical features below 2 eV is misattributed to a $CuAlO_2$ band gap. In real crystals, such experimental features are due to Cu vacancies and Al antisite defect states.[10−12]

Figure 1b shows the band structure for spin-up $|\uparrow\rangle$ and spin-down $|\downarrow\rangle$ states separately along with the associated spin-polarized DOS $CuFeO_2$. Both spin-polarizations have VB states that consist of Cu-3d orbitals. The VB maximum is located at the F-point in the Brillouin zone with a near-maximum at the L-point. By contrast, spin-polarization has a significant effect on the CB with $|\downarrow\rangle$ and $|\uparrow\rangle$ states consisting of
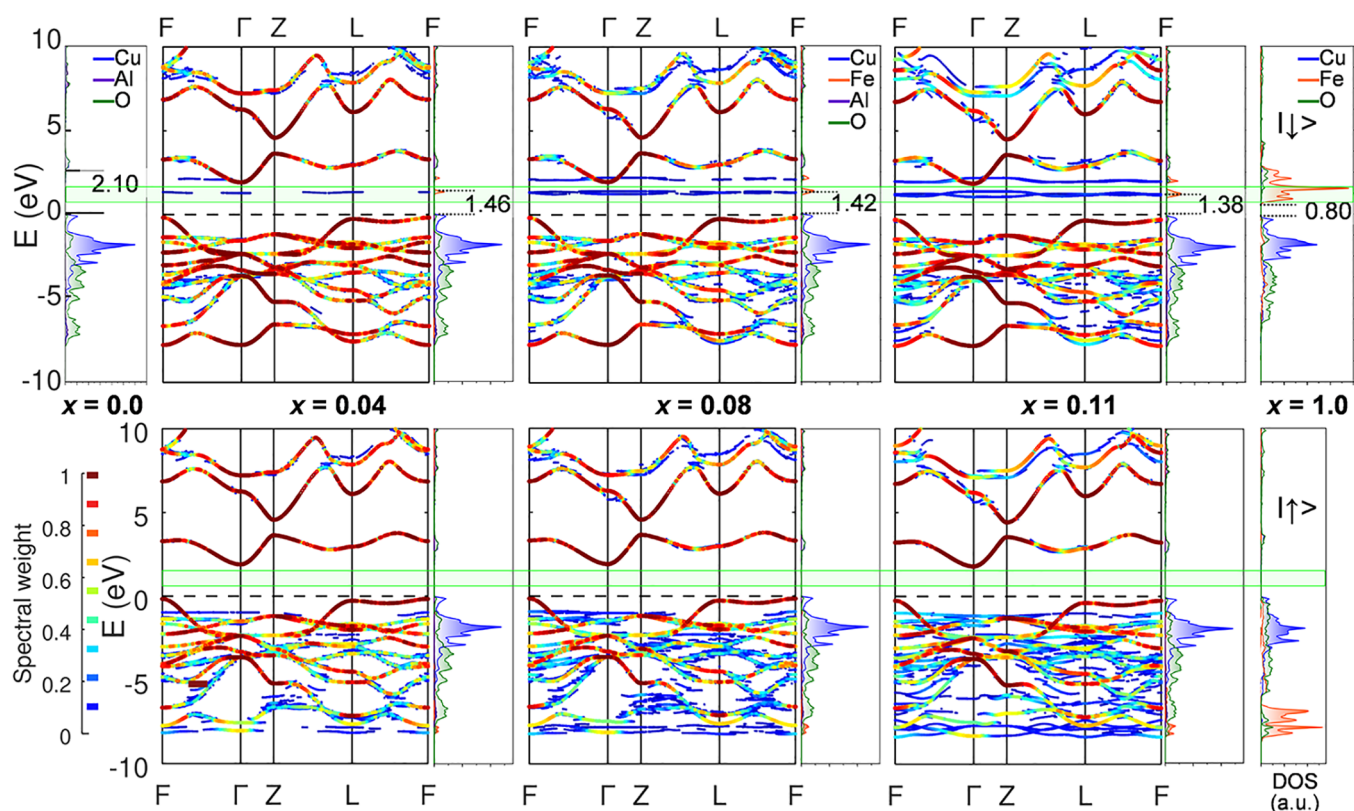
**Figure 2.** Spin-polarized electronic band structures of $CuAl_{1-x}Fe_xO_2$ for $x$ = 0.0, 0.04, 0.08, 0.11, and 1.0 and the associated density of states alongside, calculated for the supercell made of $3 \times 3 \times 3$ primitive unit cell. The arrows show the spin state of the density of states. The spectral weight scale of the colors is shown on the bottom left. The black dashed lines show the Fermi energy. Shaded rectangles highlight the energy region where the Fe-3d-related state builds.

Fe-3d and O-2p orbitals and with minima at the L- and Γ-points, respectively. Consequently, $CuFeO_2$ has spin-polarized band gaps, with an indirect $E_g$ = 0.8 eV to $|\downarrow\rangle$ states and optically allowed band gap at $E_g^{/}$ = 3.1 eV to $|\uparrow\rangle$ states. These values are consistent with reported observations of $E_g$ = 1.1 eV and two direct optical band gaps at $E_g'$ = 2.0 and 3.4 eV, respectively.[44−46] Exchanging Al for Fe significantly narrows the fundamental gap and hence is expected to change the optical properties in the visible and near-infrared regions. The shaded rectangle running horizontally across Figure 1 between energies 0.2 and 2 eV serves to accentuate the lack of calculated states in $CuAlO_2$ and the closely spaced bands present for $CuFeO_2$.

Figure 2 shows the GGA+$U$ first-principles supercell calculations of the $CuAl_{1-x}Fe_xO_2$ for $x$ = 0.04, 0.08, and 0.11. The top and bottom rows show the $|\downarrow\rangle$ and $|\uparrow\rangle$ band structures, respectively, with the associated DOS plotted alongside. For comparison, the DOS for $x$ = 0.0 and 1.0 are included (without their band structures) on the upper left and lower right for comparison across the entire Fe concentration range. The color spectrum (from white to dark red) is associated with the spectral weight from 0.0 to 1.0, which denotes both the magnitude of the corresponding Bloch character and degeneracy of the bands at any point in $k$-space when unfolding the supercell band structure onto the effective unit cell of the ternary compound.[47]

In dilute $CuAl_{1-x}Fe_xO_2$, two changes may be expected: (1) Because of breaking the inversion symmetry in $R\bar{3}m$ structure, the forbidden direct transition at Γ-point becomes allowed. However, these calculations clarify that the minimum optical transition is at the L-point, which indicates that this change should not be significant. (2) Spin-down Fe-3d states are added into the $CuAlO_2$ band gap, below the CB minimum, and can decrease the fundamental band gap. Spin-up Fe-3d orbitals are added to the VB but below VB maximum without changing the band gap. Indeed, the increase in $|\downarrow\rangle$ Fe-3d orbitals do narrow the gap, but these orbitals are not well-defined in $k$-space, so they are weak and hence have a low spectral weight (indicated by blue). Nonetheless, increasing Fe concentration increases the coverage of the blue bands throughout the band structure. Meanwhile, $|\uparrow\rangle$ Fe-3d orbitals have increased the coverage of blue bands in the VB with minimal modification to the CB band structure. Overall, the addition of band compared to $CuFeO_2$ is expected to increase the optical absorption in the visible and near-infrared. The shaded rectangle running horizontally across Figure 2 between energies 0.2 and 2 eV serves to accentuate the lack of states in the calculated $CuAlO_2$ and this buildup of states in the $CuAl_{1-x}Fe_xO_2$ alloys.

Room-temperature optical reflection ($R$) spectra were converted by using the Kubelka−Munk method for highly scattering media[48,49] into the ratio of the absorption coefficient ($\alpha$) and scattering coefficient ($S$) by using $\alpha/S = F(R_\infty) = (1 − R)^2/2R$. Figure 3a shows $F(R_\infty)$ for powdered $CuAl_{1-x}Fe_xO_2$ with $x$ = 0.0−1.0. Typically, such data have an energy-dependent background that can be seen as lifting the troughs in the spectra above $F(R_\infty)$ = 0. Figure 3b shows $F(R_\infty)$ with the background subtracted and deconvolution of the peaks with a series of Gaussians. The peaks of each feature are labeled on the $CuAlO_2$ spectra and drawn below the spectra for comparison. In the spectra, except for $x$ = 1.0, there are
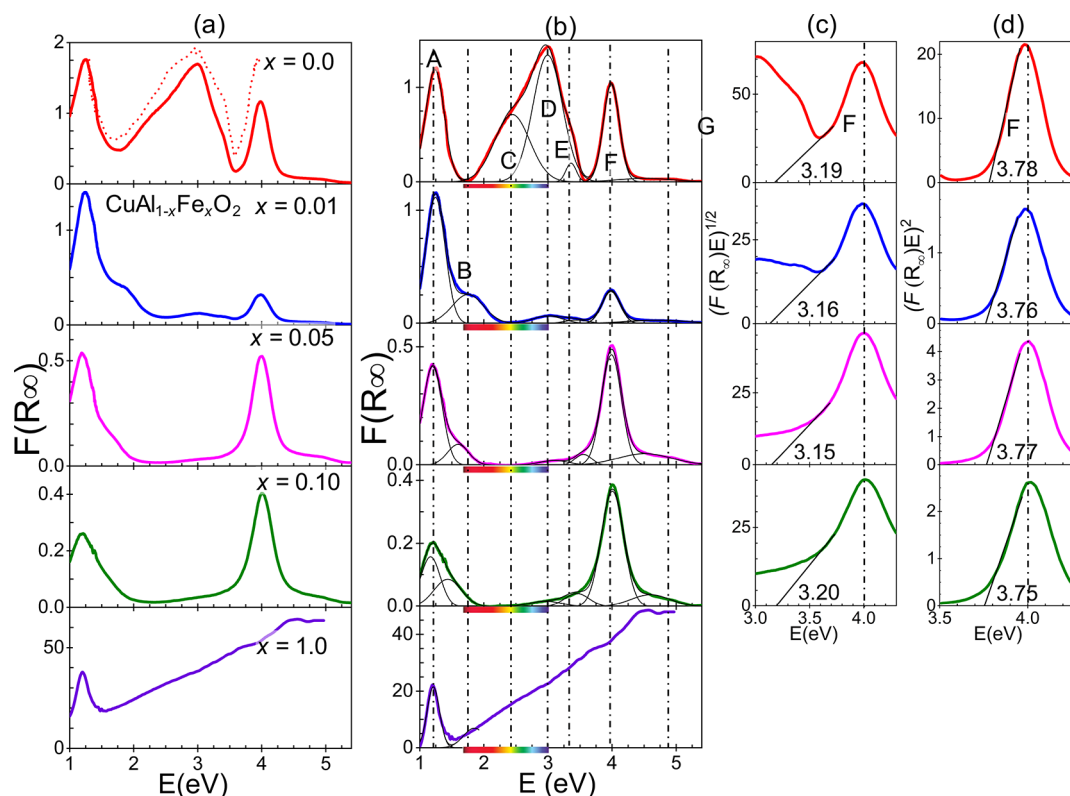
**Figure 3.** (a) Raw $F(R_\infty)$ calculated from reflection data by Kubelka−Munk theory plotted for CuAl$_{1-x}$Fe$_x$O$_2$, $x$ = 0.0−1.0; the subtracted background is shown by dashed lines. For $x$ = 0.0 we include data for a recently synthesized powder[52] (dotted). (b) $F(R_\infty)$ without the background and the fitted peaks using Gaussian functions, shown as dashed lines and labeled A−G. (c) and (d) are Tauc plots for the direct and indirect band gaps, respectively, with the fitted lines and intercepts shown.
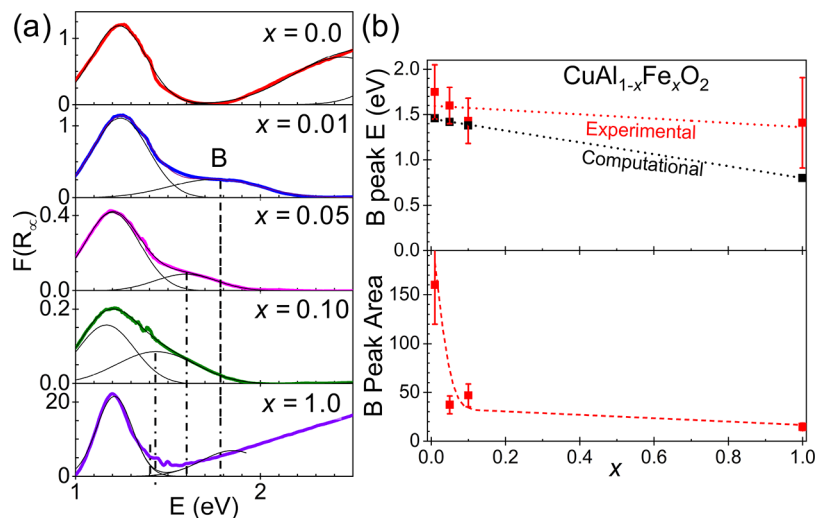


**Figure 4.** (a) Expanded view of Fe-related absorption peak (B). (b) Top: plot of the energy of the Fe-related absorption (B) and position of the Fe-related state in the modeled band structure vs $x$. (b) Bottom: plot of area under the peak for the Fe-related absorption (B). The dashed lines are the guides to the eye to follow the trend.

multiple peaks labeled A−G with increasing photon energy. The spectrum for CuFeO$_2$ ($x$ = 1.0) is distinctly different, showing a monotonic increase above peak A, with some structure above 4 eV. This increase is consistent with other studies[50,51] and is a reflection of the closely spaced bands that are present in the DFT calculations (see Figure 1).

Powder samples are known to exhibit impurities, defects, and surface states in the optical absorption that cannot be compared directly to calculations based on single crystals

without intrinsic or extrinsic defects. Previously, defect absorption peaks[14,52] have been identified and can be related to the large absorption peaks labeled A, C, D, and E. X-ray photoelectron spectroscopy indicates that these powders have a significant amount of Cu$^{2+}$ on their surfaces.[31] With that in mind, peak A at ∼1.2 eV is likely due to Cu$^{2+}$/Cu$^{+}$ intervalence transitions associated with mixed oxidation states.[53] This is consistent with the feature decreasing in strength with the addition of a little Fe. Peaks C, D, and E are probably due to

oxygen vacancies and oxygen interstitials, which also decrease in strength with Fe concentration.[14] The weak high-energy feature G is probably associated with a transition to one of the higher energy bands and not important here.

Peak F at ~4.0 eV has been identified as the direct optical band gap ($E'_g$) at the L-valley.[16,52] Figure 3c,d shows Tauc plots to determine direct and indirect ($E_g$) for $x = 0.0$, 0.01, 0.05, and 0.10. In the Tauc method,[54,55] absorption is associated with the band edge such that $[F(R_\infty)\hbar\omega]^n \propto (\hbar\omega - E'_g)$, where $\hbar$ is the reduced Planck constant, $\omega$ is the optical frequency, and the exponent is set as $n = 2$ or $1/2$ for direct or indirect transitions, respectively.[56,57] From the measurements, the fundamental gap corresponding to the indirect $F-\Gamma$ transition is ~3.8 eV, and the direct optical gap ($E'_g$) corresponding to the L-valley transition is ~3.2 eV. Both values are consistent with the calculated range of fundamental and optical band gaps, $E_g$ and $E'_g$, respectively.

The clear positive spectral indicator for the introduction of Fe into the alloy is peak B. It emerges as a shoulder on the high-energy edge of peak A in the $x = 0.01$ spectrum and remains in the $x = 0.05$ and 0.10 spectra as well. By comparison, peaks C and D are suppressed with the introduction of Fe, and the defect-related peak A and the band-edge-related peak F are both observed for the series of dilute alloys. This result is unsurprising for peak F because even at $x = 0.1$, Vegard's law predicts band gaps closer to pure $CuAlO_2$.[58] Peak B is central to this work and is indicated in Figure 4a with a close-up of the relevant spectral range.

The position of peak B in the $F(R_\infty)$ spectrum corresponds to the appearance of the $|\downarrow\rangle$ Fe-3d bands below the CB minimum in the DFT calculations in the band gap (see Figure 2). Experimentally, peak B is centered at 1.8 eV in the $x = 0.01$ spectrum and red-shifts to 1.4 eV in the $x = 0.10$ spectrum. This red-shift with Fe concentration is not observed for any other peaks shown in Figure 3b and can be compared to the position of the Fe-3d bands as a function of $x$ in Figure 2. In Figure 2, transitions between the VB maximum to the Fe-3d bands are labeled for the series of dilute alloys, also following a red-shift of the band with increasing Fe concentration. A summary of the experimentally observed peak center energies and computed transition energies is shown in the top panel of Figure 4b. The error bars are half the full width at half-maximum of peak B. The experimental (squares) and computed (circles) are fitted to linear lines (dotted). The trends of experiment and computation show good agreement and that peak B depends on the introduction of Fe and the concentration of Fe. To the best of the authors' knowledge, this is the first observation of a purely Fe-dependent mode observed in the $CuFe_xAl_{1-x}O_2$ crystal.

Finally, in the bottom panel of Figure 4b we plot the area (height times full width at half-maximum) of peak B as a function of Fe concentration. It is seen that the peak is nonexistent for $CuAlO_2$, is strong for $x = 0.01$, and generally decreases with increasing Fe concentration. The peak area decrease is slightly nonmonotonic, dipping down at $x = 0.05$ and slightly recovering at $x = 0.10$, before continuing to decrease to its ultimate area value in $CuFeO_2$. The dip at $x = 0.05$ is reminiscent of observations in delafossite Cu-$Ga_{1-x}Fe_xO_2$, where Fe is ordered in planes as the number of Fe atoms is commensurate with a large supercell and produces an additional degree of long-range order.[17] The overall decrease in the area of peak B is somewhat surprising given the increase in Fe and the buildup of the Fe-3d states (shown in Figure 2). This may be the result of powder samples, with large surface-to-volume ratios and related defects, or the ordering of Fe with increased Fe concentration.

## CONCLUSIONS

The optical reflection spectra are measured for $CuAl_{1-x}Fe_xO_2$ for $x = 0.0-1.0$ powders, and band structures are calculated by the first-principles DFT. A PBE+$U$ approach is used for the calculations, and $U$ is optimized to best match with the experimental results. According to the band structure calculations, the fundamental indirect band gap is the $F-\Gamma$ transition, experimentally observed at ~3.2 eV, and the direct optical band gap is at the L-point, observed at ~3.8 eV. Experimentally, the positions of these band gaps are insensitive to Fe content ($x = 0.01-0.10$), in agreement with the computed band structures.

The Fe concentration does result in a new optical feature near ~1.4 eV that undergoes a red-shift with increasing concentration and is associated with Fe-3d orbitals that form a band below the $CuAlO_2$ conduction band edge. Earlier work suggested alloying breaks the inversion symmetry in the $R\bar{3}m$ structure, such that the otherwise-forbidden direct transition at the $\Gamma$-point becomes allowed. However, the presented DFT calculations confirm that the minimum direct band gap remains at the L-point, ruling out that possibility. Nonetheless, the Fe-concentration-dependent optical feature can be tuned by composition and offers a new absorption mechanism near 1.6 eV in $CuAl_{1-x}Fe_xO_2$. This result may make powders of dilute-Fe delafossite alloys more appealing for applications such as photocatalytic activity.

## AUTHOR INFORMATION

### Corresponding Author
**Matthew B. Johnson** − *Department of Physics & Astronomy, West Virginia University, Morgantown, West Virginia 26506, United States*; Email: matthew.johnson@mail.wvu.edu

### Authors
**Mina Aziziha** − *Department of Physics & Astronomy, West Virginia University, Morgantown, West Virginia 26506, United States*; orcid.org/0000-0003-4001-6413

**Saeed Akbarshahi** − *Department of Physics & Astronomy, West Virginia University, Morgantown, West Virginia 26506, United States*

**Suresh Pittala** − *Department of Physics, Indian Institute of Science, Bangalore 560012, India*; orcid.org/0000-0003-3187-466X

**Sayandeep Ghosh** − *Department of Physics, Indian Institute of Technology, Guwahati, Assam 781039, India*

**Rishmali Sooriyagoda** − *Department of Physics & Astronomy, West Virginia University, Morgantown, West Virginia 26506, United States*

**Aldo H. Romero** − *Department of Physics & Astronomy, West Virginia University, Morgantown, West Virginia 26506, United States*

**Subhash Thota** − *Department of Physics, Indian Institute of Technology, Guwahati, Assam 781039, India*

**Alan D. Bristow** − *Department of Physics & Astronomy, West Virginia University, Morgantown, West Virginia 26506, United States*

**Mohindar S. Seehra** − *Department of Physics & Astronomy, West Virginia University, Morgantown, West Virginia 26506, United States*

## REFERENCES

(1) Choi, S. Y.; Kim, C.-D.; Han, D. S.; Park, H. Facilitating Hole Transfer on Electrochemically Synthesized P-Type CuAlO$_2$ Films for Efficient Solar Hydrogen Production from Water. *J. Mater. Chem. A* **2017**, *5* (21), 10165−10172.

(2) Zhao, Q.-M.; Zhao, Z.-Y.; Liu, Q.-L.; Yao, G.-Y.; Dong, X.-D. Delafossite CuGaO$_2$ as Promising Visible-Light-Driven Photocatalyst: Synthesize, Properties, and Performances. *J. Phys. D: Appl. Phys.* **2020**, *53* (13), 135102.

(3) Santra, S.; Das, N. S.; Chattopadhyay, K. K. Wide Band Gap P-Type Nanocrystalline CuBO2 as a Novel UV Photocatalyst. *Mater. Res. Bull.* **2013**, *48* (7), 2669−2677.

(4) Kato, S.; Takagi, N.; Saito, K.; Ogasawara, M. Synthesis of Delafossite-Type Ag$_{0.9}$MnO$_2$ by the Precipitation Method at Room Temperature. *ACS Omega* **2019**, *4* (6), 9763−9768.

(5) Maruyama, Y.; Irie, H.; Hashimoto, K. Visible Light Sensitive Photocatalyst, Delafossite Structured $\alpha$-AgGaO$_2$. *J. Phys. Chem. B* **2006**, *110* (46), 23274−23278.

(6) Zhao, R.-D.; Zhang, Y.-M.; Liu, Q.-L.; Zhao, Z.-Y. Effects of the Preparation Process on the Photocatalytic Performance of Delafossite CuCrO$_2$. *Inorg. Chem.* **2020**, *59* (22), 16679−16689.

(7) Kawazoe, H.; Yasukawa, M.; Hyodo, H.; Kurita, M.; Yanagi, H.; Hosono, H. P-Type Electrical Conduction in Transparent Thin Films of CuAlO2. *Nature* **1997**, *389* (6654), 939−942.

(8) Yanagi, H.; Inoue, S.; Ueda, K.; Kawazoe, H.; Hosono, H.; Hamada, N. Electronic Structure and Optoelectronic Properties of Transparent P-Type Conducting CuAlO2. *J. Appl. Phys.* **2000**, *88*, 4159.

(9) Benko, F. A.; Koffyberg, F. P. Opto-Electronic Properties of CuAlO$_2$. *J. Phys. Chem. Solids* **1984**, *45* (1), 57−59.

(10) Gillen, R.; Robertson, J. Band Structure Calculations of CuAlO2, CuGaO2, CuInO2 and CuCrO2 by Screened Exchange. *Phys. Rev. B: Condens. Matter Mater. Phys.* **2011**, *84* (3), 035125.

(11) Trani, F.; Vidal, J.; Botti, S.; Marques, M. A. L. Band Structures of Delafossite Transparent Conductive Oxides from a Self-Consistent G W Approach. *Phys. Rev. B: Condens. Matter Mater. Phys.* **2010**, *82* (8), 085115.

(12) Vidal, J.; Trani, F.; Bruneval, F.; Marques, M. A. L.; Botti, S. Effects of Electronic and Lattice Polarization on the Band Structure of Delafossite Transparent Conductive Oxides. *Phys. Rev. Lett.* **2010**, *104* (13), 136401.

(13) Tate, J.; Ju, H. L.; Moon, J. C.; Zakutayev, A.; Richard, A. P.; Russell, J.; McIntyre, D. H. Origin of p -Type Conduction in Single-Crystal CuAlO2. *Phys. Rev. B: Condens. Matter Mater. Phys.* **2009**, *80* (16), 165206.

(14) Scanlon, D. O.; Watson, G. W. Conductivity Limits in CuAlO$_2$ from Screened-Hybrid Density Functional Theory. *J. Phys. Chem. Lett.* **2010**, *1* (21), 3195−3199.

(15) Laskowski, R.; Christensen, N. E.; Blaha, P.; Palanivel, B. Strong Excitonic Effects in CuAlO 2 Delafossite Transparent Conductive Oxides. *Phys. Rev. B: Condens. Matter Mater. Phys.* **2009**, *79* (16), 165209.

(16) Pellicer-Porres, J.; Segura, A.; Gilliland, A. S.; Muñoz, A.; Rodríguez-Hernández, P.; Kim, D.; Lee, M. S.; Kim, T. Y. On the Band Gap of CuAlO2 Delafossite. *Appl. Phys. Lett.* **2006**, *88* (18), 181904.

(17) Senty, T. R.; Haycock, B.; Lekse, J.; Matranga, C.; Wang, H.; Panapitiya, G.; Bristow, A. D.; Lewis, J. P. Optical Absorption and Disorder in Delafossites. *Appl. Phys. Lett.* **2017**, *111* (1), 012102.

(18) Vojkovic, S.; Fernandez, J.; Elgueta, S.; Vega, F. E.; Rojas, S. D.; Wheatley, R. A.; Seifert, B.; Wallentowitz, S.; Cabrera, A. L. Band Gap Determination in Multi-Band-Gap CuFeO2 Delafossite Epitaxial Thin Film by Photoconductivity. *SN Appl. Sci.* **2019**, *1* (11), 1322.

(19) Nie, X.; Wei, S.-H.; Zhang, S. B. Bipolar Doping and Band-Gap Anomalies in Delafossite Transparent Conductive Oxides. *Phys. Rev. Lett.* **2002**, *88* (6), 066405.

(20) Ueda, K.; Hase, T.; Yanagi, H.; Kawazoe, H.; Hosono, H.; Ohta, H.; Orita, M.; Hirano, M. Epitaxial Growth of Transparent P-Type Conducting CuGaO2 Thin Films on Sapphire (001) Substrates by Pulsed Laser Deposition. *J. Appl. Phys.* **2001**, *89* (3), 1790.

(21) Falabretti, B.; Robertson, J. Electronic Structures and Doping of SnO$_2$, CuAlO2, and CuInO2. *J. Appl. Phys.* **2007**, *102* (12), 123703.

(22) Cohen, A. J.; Mori-Sanchez, P.; Yang, W. Insights into Current Limitations of Density Functional Theory. *Science* **2008**, *321* (5890), 792−794.

(23) Anisimov, V. I.; Zaanen, J.; Andersen, O. K. Band Theory and Mott Insulators: Hubbard $U$ Instead of Stoner $I$. *Phys. Rev. B: Condens. Matter Mater. Phys.* **1991**, *44* (3), 943−954.

(24) Gilliland, S.; Pellicer-Porres, J.; Segura, A.; Muñoz, A.; Rodríguez-Hernández, P.; Kim, D.; Lee, M. S.; Kim, T. Y. Electronic Structure of CuAlO2 and CuScO2 Delafossites under Pressure. *Phys. Status Solidi B* **2007**, *244* (1), 309−314.

(25) Jain, A.; Hautier, G.; Ong, S. P.; Moore, C. J.; Fischer, C. C.; Persson, K. A.; Ceder, G. Formation Enthalpies by Mixing GGA and GGA + U Calculations. *Phys. Rev. B: Condens. Matter Mater. Phys.* **2011**, *84* (4), 045115.

(26) Perdew, J. P.; Burke, K.; Ernzerhof, M. Generalized Gradient Approximation Made Simple. *Phys. Rev. Lett.* **1996**, *77* (18), 3865−3868.

(27) Blöchl, P. E. Projector Augmented-Wave Method. *Phys. Rev. B: Condens. Matter Mater. Phys.* **1994**, *50* (24), 17953−17979.

(28) Aziziha, M.; Motamedifar, M.; Mahdavifar, S. Multicritical Point in the One-Dimensional Quantum Compass Model. *Acta Phys. Polym., B* **2013**, *44* (2), 221.

(29) Brothers, E. N.; Izmaylov, A. F.; Normand, J. O.; Barone, V.; Scuseria, G. E. Accurate Solid-State Band Gaps via Screened Hybrid Electronic Structure Calculations. *J. Chem. Phys.* **2008**, *129* (1), 011102.

(30) Amrute, A. P.; Łodziana, Z.; Mondelli, C.; Krumeich, F.; Pérez-Ramírez, J. Solid-State Chemistry of Cuprous Delafossites: Synthesis and Stability Aspects. *Chem. Mater.* **2013**, *25* (21), 4423−4435.

(31) Aziziha, M.; Byard, S. A.; Beesely, R.; Lewis, J. P.; Seehra, M. S.; Johnson, M. B. Magnetic Properties of Fe-Doped CuAlO$_2$ and Role of Impurities. *AIP Adv.* **2019**, *9* (3), 035030.

(32) Aziziha, M.; Beesley, R.; Magers, J. R.; Mottaghi, N.; Holcomb, M. B.; Lewis, J. P.; Seehra, M. S.; Johnson, M. B. Electronic State and Concentration of Fe3+ in CuAl1-Fe O2 Determined by Magnetic Measurements. *J. Magn. Magn. Mater.* **2019**, *471*, 495−500.

(33) Aziziha, M.; Akbarshahi, S.; Ghosh, S.; Pramanik, P.; Lewis, J. P.; Romero, A. H.; Thota, S.; Seehra, M. S.; Johnson, M. B. Phonon Dynamics in Anisotropic Dilute CuAl$_{1-x}$Fe$_x$O$_2$ Delafossite Alloys by a Weighted Dynamical Matrix Approach. *J. Phys. Chem. C* **2019**, *123* (50), 30604−30612.

(34) Aziziha, M.; Akbarshahi, S.; Ghosh, S.; Pramanik, P.; Sooriyagoda, R.; Romero, A. H.; Thota, S.; Bristow, A. D.; Seehra, M. S.; Johnson, M. B. Optical Properties of Dilute CuAl1-XFexO2 Delafossite Alloys. *Frontiers in Optics/Laser Science* **2020**, *JM6A*, 31.

(35) Kresse, G.; Hafner, J. *Ab Initio* Molecular Dynamics for Liquid Metals. *Phys. Rev. B: Condens. Matter Mater. Phys.* **1993**, *47* (1), 558−561.

(36) Kresse, G.; Hafner, J. *Ab Initio* Molecular-Dynamics Simulation of the Liquid-Metal-Amorphous-Semiconductor Transition in Germanium. *Phys. Rev. B: Condens. Matter Mater. Phys.* **1994**, *49* (20), 14251−14269.

(37) Kresse, G.; Furthmüller, J. Efficiency of Ab-Initio Total Energy Calculations for Metals and Semiconductors Using a Plane-Wave Basis Set. *Comput. Mater. Sci.* **1996**, *6* (1), 15−50.

(38) Dudarev, S. L.; Botton, G. A.; Savrasov, S. Y.; Humphreys, C. J.; Sutton, A. P. Electron-Energy-Loss Spectra and the Structural Stability of Nickel Oxide: An LSDA+U Study. *Phys. Rev. B: Condens. Matter Mater. Phys.* **1998**, *57* (3), 1505−1509.

(39) Grau-Crespo, R.; Hamad, S.; Catlow, C. R. A.; de Leeuw, N. H. Symmetry-Adapted Configurational Modelling of Fractional Site Occupancy in Solids. *J. Phys.: Condens. Matter* **2007**, *19* (25), 256201.

(40) Wang, L.-W.; Bellaiche, L.; Wei, S.-H.; Zunger, A. Majority Representation" of Alloy Electronic States. *Phys. Rev. Lett.* **1998**, *80* (21), 4725−4728.

(41) Rubel, O.; Bokhanchuk, A.; Ahmed, S. J.; Assmann, E. Unfolding the Band Structure of Disordered Solids: From Bound States to High-Mobility Kane Fermions. *Phys. Rev. B: Condens. Matter Mater. Phys.* **2014**, *90* (11), 115202.

(42) Yu, R.-S.; Liang, S.-C.; Lu, C.-J.; Tasi, D.-C.; Shieu, F.-S. Characterization and Optoelectronic Properties of P-Type N-Doped CuAlO2 Films. *Appl. Phys. Lett.* **2007**, *90* (19), 191117.

(43) Banerjee, A. N.; Chattopadhyay, K. K. Recent Developments in the Emerging Field of Crystalline P-Type Transparent Conducting Oxide Thin Films. *Prog. Cryst. Growth Charact. Mater.* **2005**, *50* (1−3), 52−105.

(44) Benko, F. A.; Koffyberg, F. P. Opto-Electronic Properties of p- and n-Type Delafossite, CuFeO2. *J. Phys. Chem. Solids* **1987**, *48* (5), 431−434.

(45) Deng, Z.; Fang, X.; Wu, S.; Dong, W.; Shao, J.; Wang, S.; Lei, M. The Morphologies and Optoelectronic Properties of Delafossite CuFeO2 Thin Films Prepared by PEG Assisted Sol-Gel Method. *J. Sol-Gel Sci. Technol.* **2014**, *71* (2), 297−302.

(46) Ong, K. P.; Bai, K.; Blaha, P.; Wu, P. Electronic Structure and Optical Properties of AFeO$_2$ (A = Ag, Cu) within GGA Calculations. *Chem. Mater.* **2007**, *19* (3), 634−640.

(47) Boykin, T. B.; Kharche, N.; Klimeck, G.; Korkusinski, M. Approximate Bandstructures of Semiconductor Alloys from Tight-Binding Supercell Calculations. *J. Phys.: Condens. Matter* **2007**, *19* (3), 036203.

(48) Kubelka, P.; Munk, F. Ein Beitrag Zur Optik Der Farbanstriche. *Zeit. Für Tekn. Physik 12*, 593−601.

(49) Yang, L.; Miklavcic, S. J. Revised Kubelka-Munk Theory III A General Theory of Light Propagation in Scattering and Absorptive Media. *J. Opt. Soc. Am. A* **2005**, *22* (9), 1866.

(50) Oh, Y.; Yang, W.; Kim, J.; Jeong, S.; Moon, J. Enhanced Photocurrent of Transparent CuFeO$_2$ Photocathodes by Self-Light-Harvesting Architecture. *ACS Appl. Mater. Interfaces* **2017**, *9* (16), 14078−14087.

(51) Xiong, D.; Zhang, Q.; Verma, S. K.; Bao, X.-Q.; Li, H.; Zhao, X. Crystal Structural, Optical Properties and Mott-Schottky Plots of p-Type Ca Doped CuFeO 2 Nanoplates. *Mater. Res. Bull.* **2016**, *83*, 141−147.

(52) Guarneros Aguilar, C.; Estrada Moreno, C.; Pacio Castillo, M.; Caballero-Briones, F. Effect of Calcination Temperature on Structure and Thermoelectric Properties of CuAlO2 Powders. *J. Mater. Sci.* **2018**, *53* (3), 1646−1657.

(53) Tangcharoen, T.; T-Thienprasert, J.; Kongmark, C. Effect of Calcination Temperature on Structural and Optical Properties of MAl2O4 (M = Ni, Cu, Zn) Aluminate Spinel Nanoparticles. *J. Adv. Ceram.* **2019**, *8* (3), 352−366.

(54) Tauc, J.; Grigorovici, R.; Vancu, A. Optical Properties and Electronic Structure of Amorphous Germanium. *Phys. Status Solidi B* **1966**, *15* (2), 627−637.

(55) Meymian, M. R. Z.; Heravi, A. D.; Mehr, A. K. Influence of Bias Voltage on Optical and Structural Characteristics of Cu3N Films Deposited by Reactive RF Magnetron Sputtering in a Pure Nitrogen Atmosphere. *Materials Science in Semiconductor Processing* **2020**, 7.

(56) Sivaneri, K. V. I.; Ozmen, O.; Aziziha, M.; Sabolsky, E. M.; Evans, T. H.; DeVallance, D. B.; Johnson, M. B. Robust Polymer-HfO$_2$ Thin Film Laminar Composites for Tactile Sensing Applications. *Smart Mater. Struct.* **2019**, *28* (2), 025002.

(57) Zamani Meymian, M. R.; Haji Abdolvahab, R.; Kosari Mehr, A. Fractal Characteristics of TiO$_2$-Ag Nanocomposite Films Deposited by a Grid-Assisted Co-Sputtering Method. *Appl. Surf. Sci.* **2019**, *480*, 593−600.

(58) Lekse, J. W.; Underwood, M. K.; Lewis, J. P.; Matranga, C. Synthesis, Characterization, Electronic Structure, and Photocatalytic Behavior of CuGaO$_2$ and CuGa$_{1-x}$Fe$_x$O$_2$ (x = 0.05, 0.10, 0.15, 0.20) Delafossites. *J. Phys. Chem. C* **2012**, *116* (2), 1865−1872.

G